Heliyon 9 (2023) e21974

Contents lists available at ScienceDirect

Heliyon

journal homepage: www.cell.com/heliyon

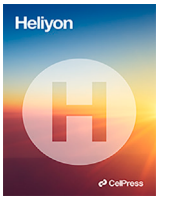

Research article

Infrared Raman spectroscopy enables noninvasive biochemical assessment of skin tissue and the thermal stability

Xiaoyi Wang [a], Fangqi Hua [b], Xianhai Xie [c], Yungang Wu [a], Wenxue Sun [d], Zipei Jiang [e], Jinzhong Zhang [b,*], Xu Luo [f,g,h,**]

[a] *Traditional Chinese Medicine (TCM) Orthopedics & Traumatology, the First Affiliated Hospital of Wenzhou Medical University, Wenzhou 325000, Zhejiang, China*

[b] *Department of Wound Repair, the Quzhou Affiliated Hospital of Wenzhou Medical University, Quzhou People's Hospital, Quzhou 324000, China*

[c] *Department of the Trauma, the First Affiliated Hospital of Wenzhou Medical University, Wenzhou 325000, Zhejiang, China*

[d] *Hemodialysis Room, Department of Nephrology, the First Affiliated Hospital of Wenzhou Medical University, Wenzhou 325000, Zhejiang, China*

[e] *Department of Ophthalmology, the First Affiliated Hospital of Wenzhou Medical University, Wenzhou 325000, Zhejiang, China*

[f] *National Key Clinical Specialty (Wound Healing), Department of Wounds and Burns, the First Affiliated Hospital of Wenzhou Medical University, Wenzhou 325000, Zhejiang, China*

[g] *Key Laboratory of Intelligent Treatment and Life Support for Critical Diseases of Zhejiang Province, the First Affiliated Hospital of Wenzhou Medical University, Wenzhou 325000, China*

[h] *Zhejiang Engineering Research Center for Hospital Emergency and Process Digitization, Wenzhou 325000, Zhejiang, China*

ARTICLE INFO

Keywords:
Raman spectra
Skin tissue
Thermal stability
Burn injury

ABSTRACT

Raman-active modes of human skin and pork belly have been studied systematically by a near-infrared Raman spectrometer with an exciting laser of 1064 nm. The main components and quantitative determination of pork belly are extracted by fitting the Raman spectra with the normalized Raman spectra of biochemical reagents such as collagen, elastin, triolein, fibronectin, fibrin, and hyaluronic acid. It demonstrates that the main components and quantity are various at different locations of pork belly, while the main components of human skin are similar to those of pig skin. In a further step, the evolution of the heating time-dependent Raman modes of isolated pig skin has been investigated for the mechanism of burnt skin. One can find that the spatial structure and main components of skin have an excellent thermal stability in the temperature range from -120 to 200 °C, which is confirmed by the temperature dependent Raman spectra of isolated pig skin, microporous acellular dermal matrix (MADM) as well as their corresponding biochemical reagents (collagen, elastin, triolein, etc.). These results help understand the mechanism of the living skin burnt by fire or hot water, and supplies an alternative technology for surgeons to diagnose the depth of a burn injury in time.

1. Introduction

Raman spectroscopy is an optical technique, which utilizes inelastic scattering of light to identify biological tissues [1–4]. It can be applied to probe the vibrations of chemical functional groups in diverse materials such as polymers [5,6], pharmaceuticals

* Corresponding author.

** Corresponding author at: National Key Clinical Specialty (Wound Healing), Department of Wounds and Burns, the First Affiliated Hospital of Wenzhou Medical University, Wenzhou 325000, Zhejiang, China.

E-mail addresses: zjzwsy@126.com (J. Zhang), luoxu@wmu.edu.cn (X. Luo).

https://doi.org/10.1016/j.heliyon.2023.e21974
Received 31 July 2023; Received in revised form 31 October 2023; Accepted 1 November 2023

Available online 8 November 2023

[7–9], and semiconductors/insulators [10–13]. This technique provides chemical fingerprinting services for almost materials except the chemical information [13–15]. Besides, the frequency of exit photon (laser wavelength) is one of the important parameters. For polymer materials, the background fluorescence will be suppressed using the Raman spectrometer equipped with a near-infrared laser source [3]. Sometimes, the Raman signals detected from the surface of tissue/cells are very weak or are challenging to identify components. A so-called surface-enhanced Raman spectroscopy has been developed, which can realize an ultrahigh sensitivity down to the single-molecule level [16,17]. Moreover, a handheld Raman spectrometer with 1064 nm excitation is prominent because it can be used in the clinical diagnosis in the near future [18,19].

Generally, there are two stages for the case of skin burns by fire or hot water. The first stage is the moment that the living skin is suffering from fire/hot water, and the extrinsic factors (temperature, contact time, pressure, specific heat capacity, etc.) are dominant [20]. The features are that it occurs suddenly, and it is all over in a matter of a few seconds. In this stage, it is a challenge for a surgeon to give an accurate initial diagnosis of the depth of a burn injury accurately by the naked eye (visual assessment) especially the superficial partial thickness and deeper partial-thickness burns, which have distinct differences in treatment, healing time, prognosis and outcome [21,22]. The second one is the post-burn stage and the intrinsic factors (immune system, inflammatory mediators, etc.) are dominant. The determination of burn depth becomes much more reliable [23]. The injury causes inflammatory mediators to be released from cells within the immune system. The mediators will cause the skins blood vessels to dilate or expand, which will allow more blood flow to the skin surface [24]. Blisters are common in superficial second-degree burns, and the blisters are caused by capillaries in the dermis leaking fluid, which pushes and lifts the epidermis [25]. During an inflammatory process, there coexists damage and repair of tissue cells. For superficial (first degree) and superficial partial thickness, the collagen structure survives and the repair of damaged tissue cells is dominant. On the other hand, collagen structure has been collapsed for deep partial thickness and full thickness (third degree) [26]. After the inflammatory factors act on the body, it causes damage tissue cells and makes the local tissue cells show degeneration and necrosis, which is required excision and grafting within 3-4 weeks [27,22]. It should be emphasized that the initial diagnosis of burn depth is very essential and difficult for both clinicians and patients.

In this study, we try to supply a spectroscopy technique to help surgeons determine the degree of burn depth at the first stage. The isolated samples have been investigated in order to avoid the effects of inflammatory reaction. The main components and quantity are various at different locations of pork belly, while the main components of human skin are similar to those of pig skin. Moreover, the temperature dependent Raman spectra of isolated pig skin indicate that the spatial structure and main components of pig skin have an excellent thermal stability in the temperature range of -120 and 200 °C.

2. Experimental section

2.1. Pork belly, pig skin and components

Analytical grade ethanol (CH_3CH_2OH, 99.7%), acetone (CH_3COCH_3, 99.5%), and isopropanol ($CH_3CH_2OHCH_3$, 99.5%) were purchased from Jiangsu YongHua Fine Chemical Reagent Co., Ltd. The biomaterials triolein ($C_{57}H_{104}O_6$ Tokyo Chemical Industry, Shanghai), bovine collagen (Sigma-Aldrich), bovine elastin (Sigma-Aldrich), hyaluronic acid (MedChemExpress), fibronectin (Sigma-Aldrich) and fibrin (Sigma-Aldrich) were purchased for detecting the main components of dermis tissues. A healthy pig (25 kg, provided by the Animal Experimental Center of Wenzhou Medical University) was killed under proper ethical protocols. We obtained the pork belly and prepared the microporous porcine acellular dermal matrix (MPADM), which has been reported elsewhere [28,29]. In brief, the 0.3 mm-thick dermis was collected once the top 0.2 mm-thick portion of the skin was excised using a motor dermatome. The pore matrix with the pore size (~135 μm) and pore space (~1.0 mm) is realized using a laser punch controlled by a computer system. In addition, the present burn wounds of isolated pig skin were generated using an ethanol-burn model with various burning times [30]. Note that the pork belly, pig skin and subcutaneous tissue used in this experiment are all isolated tissues.

2.2. Raman measurement

A Raman spectrometer is utilized to collect the Raman spectra of human/pig skin tissue with an exciting laser wavelength of 1064 nm. The integration times and irradiation powers are 10 s and 400 mW, respectively. It should be emphasized that an appropriate laser power density must be considered in clinics to avoid skin injury. The wavenumber range of spectra is 250-2000 cm^{-1} and the collection time for each spectrum was around 30 s. Moreover, a total of three spectra were collected from three different points across the surface of tissues and then averaged. Raman spectra were also collected for the pure biochemical reagents (collagen, triolein, elastin, fibronectin, fibrin and hyaluronic acid). The Raman spectra $f(\nu)$ of the epidermis/dermis/subcutaneous tissues were fitted by the normalized Raman spectra $g_i(\nu)$ of biochemical reagents with different weight index (a_i): $f(\nu) = \sum a_i g_i(\nu)$. The isolated pig skins were burnt by pure liquid ethanol with a gauze in 0, 5, 15, 30, and 45 s. The temperature dependent Raman spectra of tissues/biomaterials were carried out in a Lincam chamber from -120 to 200 °C protected by nitrogen. Note that background fluorescence in the Raman spectra was not removed and the experimental data were not mathematical smoothed.

3. Results and discussion

3.1. Raman modes of human and pig skin

Fig. 1 shows the photographs of (a) human skin from the underside of forearm, (b) pig skin and (c) subcutaneous tissue. And the corresponding Raman spectra were collected at room temperature (cf. Fig. 1d). Interestingly, the shape of spectra is similar compared

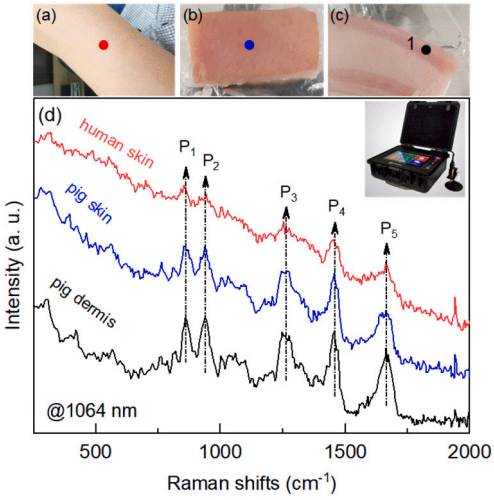

Fig. 1. Photographs of (a) human skin, (b) pig skin and (c) subcutaneous tissue, and (d) the corresponding Raman spectra measured at room temperature. Inset: the utilized Raman spectrometer. Note that the five main Raman peaks (P_1-P_5) are labeled.

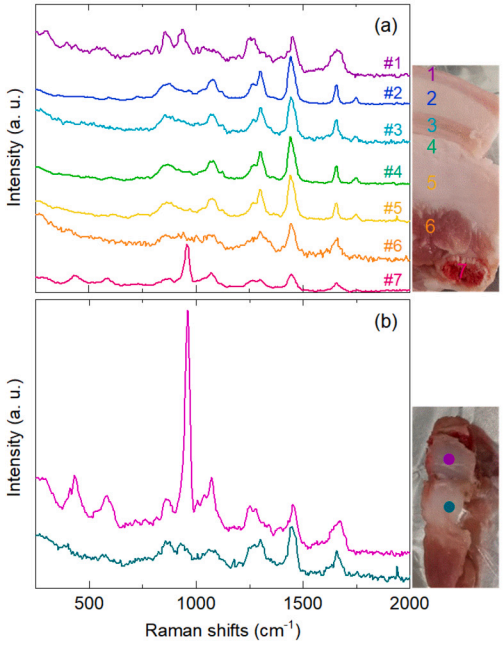

Fig. 2. (a) Raman spectra of pork belly with different layers and cross section of bone labelled from 1 to 7. (b) Raman spectra of the bone surface and nearby periosteum. Note that each spectrum is shifted in intensity for clarity.

to human and pig skin/subcutaneous tissue. There are five main Raman peaks (P_1-P_5) nearby 860, 940, 1270, 1460, and 1665 cm^{-1}, which are labeled by arrows. In addition, the spectra were fitted by multiple Lorentz functions. It was found that the peak positions and broadening are almost the same. Moreover, the intensity of Raman modes of pig skin is much larger than that of human skin. In this case, we will investigate the Raman spectra of pig dermis tissue instead of those of human skin. It indicates that the laser 1064 nm can detect the change information about dermis injury through the epidermis. Extracted the content changing trends of biochemicals in different degrees of burns by fitting the Raman spectra of burns of pig tissues. We will try to establish a relationship between normal/burnt skin and the concentration of tissue biochemicals in the following sections.

3.2. Raman-active modes of park belly

In Fig. 2a, the Raman spectra of park belly with different cells/tissues were recorded at room temperature. For the case of dermis tissue (# 1), there are double peaks nearby 850 and 950 cm^{-1}. The width at half-maximum of the Raman peaks is broad compared to the other Raman spectra of tissues such as fat and muscle. Moreover, the Raman-active modes from the subcutaneous tissues (# 2-5)

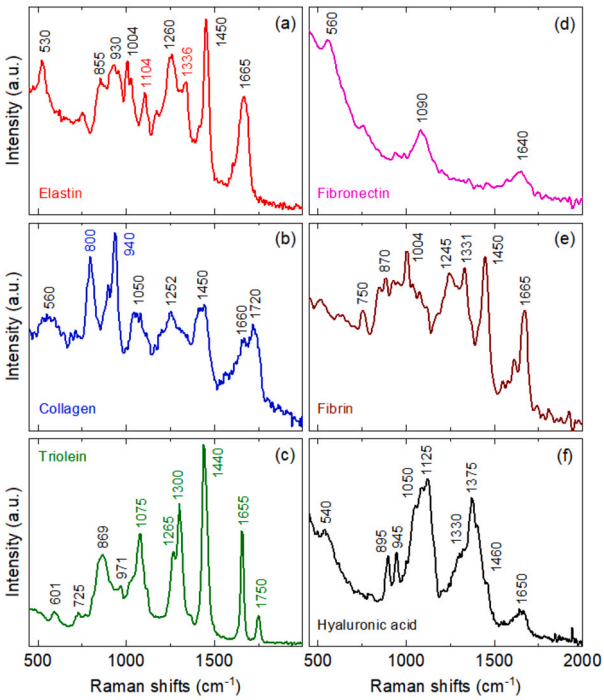

Fig. 3. Raman spectra of the pure biochemicals: (a) elastin, (b) collagen, (c) triolein, (d) fibronection, (e) fibrin, and (f) hyaluronic acid.

are sharp and have a similar feature, which means they have almost the same biochemicals. On the other hand, the Raman spectrum (# 6) comes from the muscle tissue. The intensity becomes weak and the width at half-maximum increases compared to those of fat cells. Obviously, there is an additional Raman peak at around 960 cm^{-1} in the spectrum of cross section of bone (# 7), which is attributed to the PO_4^{3-} symmetric stretches in $Ca_{10}(PO_4)_6(OH)_2$ (calcium hydroxyapatite) [31]. Besides, we measured the Raman scattering of the bone surface and nearby periosteum, as shown in Fig. 2b. It reveals that the peak nearby 960 cm^{-1} is very sharp because the density of bone cell is high. In addition, the components of periosteum are similar to those of dermis because the Raman peak positions have almost the same feature. However, the difference of peak intensities and shape reveal that the concentration of biochemicals is different.

In order to assess the main components in the skins of human and pork belly. We have investigated the pure biochemicals (elastin, collagen, triolein, fibronectin, fibrin, and hyaluronic acid) in detail by using Raman spectra measured at room temperature (Fig. 3). The molecular vibrations of elastin and the peak positions of main Raman modes are labeled in Fig. 3a. The bands at 855 and 930 cm^{-1} can be attributed to the C-C stretching vibrations of proline. And the peak at 1004 cm^{-1} can be assigned to phenylalanine. The 1104 and 1336 cm^{-1} bands are attributed to isodesmosine/desmosine, which is specific for Elastin [31]. The intense peak located at 1450 cm^{-1} is assigned to the CH_2/CH_3 bending modes of proteins [32]. Generally, the band nearby 1260 cm^{-1} comes from the amide III (C-H stretching vibration, α-helix) [33]. The band at around 1665 cm^{-1} is attributed to the amide I (C = O stretching vibrations) of structural proteins with the secondary structure of β-sheet [34,35]. Note that the ratio of the Raman intensity of the amide III and amide I suggests the evolution of the damage/repair process [36]. Fig. 3b depicts the Raman scattering of another essential protein (collagen). The unique feature of collagen is the Raman modes appeared at 800 and 940 cm^{-1}, which may originate from the hydroxyproline/proline [13]. In addition, there are some other bands related to the amide I/III, C-C or C-H bending vibrations and so on. For the case of triolein, there are dominated by C-C stretching, $=CH$, $-(CH_2)_n-$ and $-CH_3$ deformations bands (1075, 1265, 1300, and 1440 cm^{-1}), an unsaturated C = C stretching band (1655 cm^{-1}), and an ester band (C = O stretching vibrations, 1750 cm^{-1}) [37]. In Fig. 3d, the Raman bands of fibronection nearby 1090 and 1640 cm^{-1} can be attributed to the C-N stretching and amide I (β-sheet), respectively. Note that the background fluorescence of this kind of protein is more energetic, and the frequency of amide I has a shift towards lower wave numbers. Also the Raman spectra of the pure fibrin and hyaluronic acid are shown in Figs. 3e and 3f, respectively.

In order to ascertain the components of the pork belly at different positions. All the Raman spectra of pork belly (dots) were fitted with the basis Raman spectra of pure biochemicals (solid lines) using nonnegative least-squares minimization fit (cf. Fig. 4). It suggests that the Raman spectrum of each morphologic structure (#1-7) is well described using the biochemical basis spectra. For each morphologic structure, the contribution of each biochemical component was obtained (Table 1). Note that all the Raman spectra are normalized before fitting. Generally, each cell/tissue is composed largely of one or two major biochemical components, combined with some less abundant biochemicals. The weighting factor of collagen (0.175) in dermis (# 1) is dominant than other tissues (# 2-7). Obviously, triolein is dominant in fat cells/tissue. Moreover, the muscle cells/tissue include triolein, fibronection, elastin, fibrin, etc. While, the bone contains fibrin and triolein besides the main component of calcium hydroxyapatite. It is reported

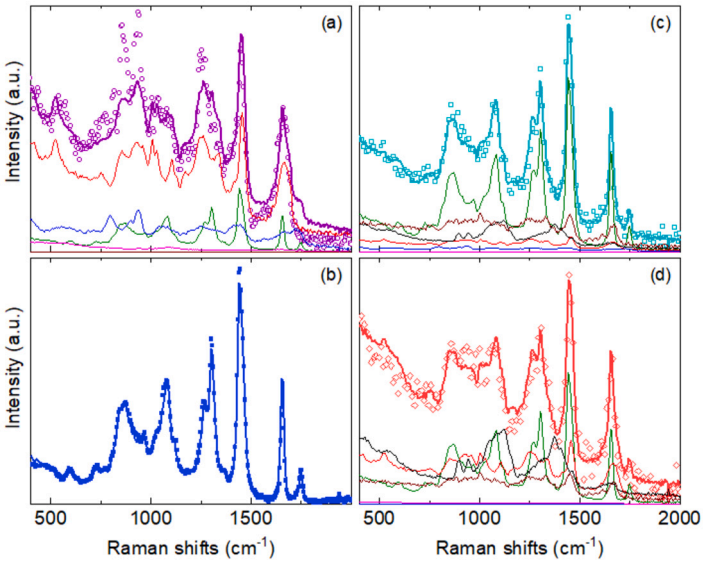

Fig. 4. Experimental data of tissue and fitted curves based on the pure biochemicals: (a) dermis tissue (#1), (b) fat tissue (#2), (c) mixture of fat and muscle (#3) and (d) muscle tissue (#6).

Table 1
The component of pork belly at different locale positions from epidermis to bone labelled from 1 to 7 in Fig. 2. (fibronection: fibro., hyaluronic acid: HA.)

	triolein	elastin	collagen	fibro.	fibrin	HA
#1	0.264	0.689	0.175	0.045	—	—
#2	0.943	—	—	—	—	—
#3	0.742	0.075	0.025	0.156	0.191	—
#4	0.929	—	—	—	0.007	0.004
#5	0.861	—	0.025	—	0.032	0.036
#6	0.453	0.258	—	0.304	0.126	0.006
#7	0.271	0.043	0.008	0.073	0.137	—

that the water content of the skin is about 25 mass% [9]. Unfortunately, the percentage of proteins, fat, and amine acid are not reported in the literatures.

3.3. Raman-active modes of pork belly burnt by ethanol

The evolution of Raman modes of isolated pig skin burnt in air for different times (0, 5, 15, 30, and 45 s) has been investigated, as shown in Fig. 5a. The main first-order Raman active modes are labeled from P_1 to P_5. The shape of curves and peak positions of main Raman-active modes are almost the same. It indicates that the biochemical structure of the skin does not be destroyed by the heat. To a certain degree, the isolated pig skin has an excellent thermal stability. Noted that the intensity of Raman modes for burnt skin increases compared to the original one. For the Raman mode (P_1) nearby 881 cm^{-1}, the intensity increases with increasing the burnt time. While other four modes (P_2-P_5) have a maximum for the case of 30 s (cf. Fig. 5b). The phenomenon can be attributed to the density increasement of the tissue due to the absorption of heat. The contact time (30 s) is a critical index for the determination of accurate initial diagnosis in time.

In a further step, temperature dependences of the isolated pig skin, microporous acellular dermal matrix, as well as their main biomaterials (i.e., collagen and elastin) have been studied in the temperature range from -120 to 200 °C in a Linkam chamber protected by nitrogen, as shown in Fig. 6. As the temperature increases, the Raman intensity of an isolated pig skin increases till about 20 °C and then decreases (cf. Fig. 6b). The shape and peak positions do not change a lot, which means the tissue/molecular structure does not have a noticeable change. For the case of microporous porcine acellular dermal matrix, the Raman intensity decreases first and then increases due to the background fluorescence. The intensity and positions do not change obviously, as shown in Fig. 6d. It is interesting that the intensities of Raman modes for pig skin are the strongest at around room temperature. On the contrast, the intensities of those for microporous porcine acellular dermal matrix are the weakest at around room temperature. Besides, we investigate the thermal stability of the main biomaterials such as collagen and elastin, as illustrated by Figs. 6e and 6f, respectively. For the elastin, the intensity has a slight increasement especially for the modes located at 800-1100 cm^{-1}, which are related to the C-C vibrations. In the temperature range of -120 to 200 °C, the isolated pig skin and microporous porcine acellular dermal matrix as well as their main components exhibit an excellent thermal stability.

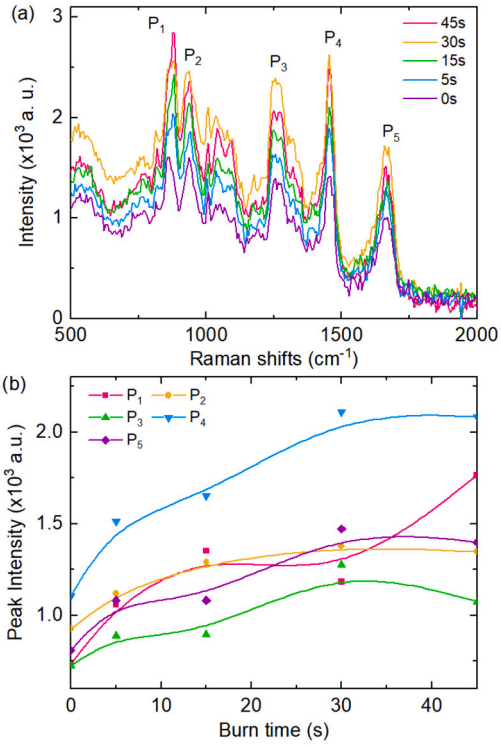

Fig. 5. (a) Raman spectra of the pig skin burnt in air by ethanol with different time of 0 – 45 s. The five main Raman peaks (P_1-P_5) are labeled. (b) The corresponding intensity of Raman modes labelled by P_i (i = 1, 2, 3, 4, and 5) as a function of burnt time.

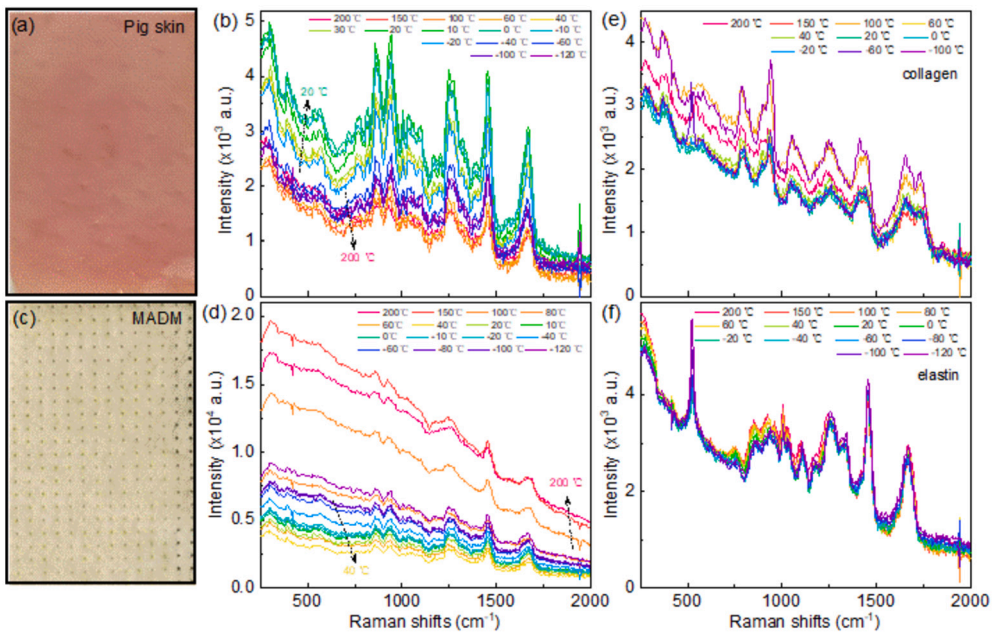

Fig. 6. Temperature dependent Raman spectra of (a, b) the isolated pig skin, (c, d) microporous acellular dermal matrix (MADM), (e) collagen, and (f) elastin powder at various temperatures from -120 to 200 °C upon heating.

4. Conclusions

In summary, the Raman active modes of isolated pig skin are investigated instead of human skin since the shape of the Raman spectra of human and pig skin are similar. The frequency, intensity and broadening of the first-order Raman-active modes are various

due to the different tissues of pork belly. By fitting the Raman spectra with the normalized Raman spectra of biochemical reagents, the main components and the corresponding contents of different cell/tissue are identified. To a certain degree, the frequency of the Raman modes does not change obviously with increasing the heating time and temperature. It means that the isolated pig skin, microporous porcine acellular dermal matrix as well as their main components exhibit an excellent thermal stability in the temperature range of -120 to 200 °C. That is the reason why surgeons have to confirm the determination of the initial diagnosis 24 h later. Therefore, Raman spectroscopy can help surgeons/clinicians to have a more accurate initial diagnosis in time, which is a much more important part for the following right treatments of burn injuries. Moreover, it also can help us to probe the evolution of chronic wound based on the change trends of components inside.

Ethics approval and consent to participate

This study was reviewed and approved by the Ethics Committee in Laboratory Animal of the First Affiliated Hospital of Wenzhou Medical University (Ethics approval number: 2021-0282). Human skin photos are provided by the volunteer (Jinzhong Zhang), who is a co-author of this paper.

CRediT authorship contribution statement

Xiaoyi Wang: Writing – original draft, Investigation, Data curation, Conceptualization. **Fangqi Hua:** Investigation, Formal analysis, Data curation. **Xianhai Xie:** Resources, Investigation, Data curation. **Yungang Wu:** Methodology, Formal analysis, Data curation, Conceptualization. **Wenxue Sun:** Resources, Methodology, Data curation, Conceptualization. **Zipei Jiang:** Methodology, Investigation, Formal analysis, Data curation, Conceptualization. **Jinzhong Zhang:** Writing – review & editing, Supervision, Investigation, Funding acquisition, Data curation. **Xu Luo:** Funding acquisition.

Declaration of competing interest

The authors declare that they have no known competing financial interests or personal relationships that could have appeared to influence the work reported in this paper.

Data availability

Data associated with the study has not been deposited into a publicly available repository and data will be made available on request.

Acknowledgements

X. Wang and F. Hua contributed equally to this work. This work was financially supported by the Project of Zhejiang Medical and Health Science and technology plan (Nos. 2022496777), the Project of Zhejiang Medical and Health Science and technology plan (Nos. 2018KY124.), and the Project of Flexible Talent Introduction (RXRC202101).

References

[1] L.A. Jakob, W.M. Deacon, Y. Zhang, B. de Nijs, E. Pavlenko, S. Hu, C. Carnegie, T. Neuman, R. Esteban, J. Aizpurua, J.J. Baumberg, Giant optomechanical spring effect in plasmonic nano- and picocavities probed by surface-enhanced Raman scattering, Nat. Commun. 14 (1) (2023) 3291, https://doi.org/10.1038/s41467-023-38124-1.

[2] A. Goel, D. Tsikritsis, N.A. Belsey, R. Pendlington, S. Glavin, T. Chen, Measurement of chemical penetration in skin using stimulated Raman scattering microscopy and multivariate curve resolution-alternating least squares, Spectrochim. Acta, Part A, Mol. Biomol. Spectrosc. 296 (2023) 122639, https://doi.org/10.1016/j.saa.2023.122639.

[3] U. Utzinger, D.L. Heintzelman, A. Mahadevan-Jansen, A. Malpica, M. Follen, R. Richards-Kortum, Near-infrared Raman spectroscopy for in vivo detection of cervical precancers, Appl. Spectrosc. 55 (8) (2001) 955–959, http://as.osa.org/abstract.cfm?URI=as-55-8-955.

[4] P. Crow, N. Stone, C.A. Kendall, J.S. Uff, J.A.M. Farmer, H. Barr, M.P.J. Wright, The use of Raman spectroscopy to identify and grade prostatic adenocarcinoma in vitro, Br. J. Cancer 89 (1) (2003) 106–108, https://doi.org/10.1038/sj.bjc.6601059.

[5] A. Gopanna, R.N. Mandapati, S.P. Thomas, K. Rajan, M. Chavali, Fourier transform infrared spectroscopy (FTIR), Raman spectroscopy and wide-angle x-ray scattering (WAXS) of polypropylene (PP)/cyclic olefin copolymer (COC) blends for qualitative and quantitative analysis, Polym. Bull. 76 (8) (2019) 4259–4274, https://doi.org/10.1007/s00289-018-2599-0.

[6] J. Casado, S. Patchkovskii, M. Zgierski, L. Hermosilla, C. Sieiro, M. Moreno Oliva, J. López Navarrete, Raman detection of ambiguous conjugated biradicals: rapid thermal singlet-to-triplet intersystem crossing in an extended viologen, Angew. Chem., Int. Ed. 120 (8) (2008) 1465–1468, https://doi.org/10.1002/ange.200704398.

[7] M.I. Sanhueza, M.F. Melendrez, C. von Plessing, C.Y. Bastidas, J.Y. Neira, J. Freer, R.d.P. Castillo, Raman microimaging as an analytical technique for simultaneous quantification and localization of active principles in pharmaceutical solid dosage forms, J. Raman Spectrosc. 51 (4) (2020) 649–659, https://doi.org/10.1002/jrs.5833.

[8] H. Nadeem, T.J. Heindel, Review of noninvasive methods to characterize granular mixing, Powder Technol. 332 (2018) 331–350, https://doi.org/10.1016/j.powtec.2018.03.035.

[9] M. Egawa, Raman microscopy for skin evaluation, Analyst 146 (4) (2021) 1142–1150, https://doi.org/10.1039/D0AN02039G.

[10] S.-Y. Ding, J. Yi, J.-F. Li, B. Ren, D.-Y. Wu, R. Panneerselvam, Z.-Q. Tian, Nanostructure-based plasmon-enhanced Raman spectroscopy for surface analysis of materials, Nat. Rev. Mater. 1 (2016) 16021, https://doi.org/10.1038/natrevmats.2016.36.

[11] A. Taghizadeh, U. Leffers, T.G. Pedersen, K.S. Thygesen, A library of ab initio Raman spectra for automated identification of 2D materials, Nat. Commun. 11 (1) (2020) 3011, https://doi.org/10.1038/s41467-020-16529-6.
[12] Y. Sun, W. Xu, X. Fu, Z. Sun, J. Wang, J. Zhang, D. Rosenbach, R. Qi, K. Jiang, C. Jing, Z. Hu, X. Ma, J. Chu, Evaluation of lattice dynamics, infrared optical properties and visible emissions of hexagonal GeO_2 films prepared by liquid phase deposition, J. Mater. Chem. C 5 (48) (2017) 12792–12799, https://doi.org/10.1039/c7tc04108j.
[13] L. Shan-Yang, L. Mei-Jane, C. Wen-Ting, FT-IR and Raman vibrational microspectroscopies used for spectral biodiagnosis of human tissues, Spectrosc. Int. J. 21 (1) (2007) 1–30, https://doi.org/10.1155/2007/278765.
[14] Y. Oshima, T. Haruki, K. Koizumi, S. Yonezawa, A. Taketani, M. Kadowaki, S. Saito, Practices, potential, and perspectives for detecting predisease using Raman spectroscopy, Int. J. Mol. Sci. 24 (15) (2023) 12170, https://doi.org/10.3390/ijms241512170.
[15] R. Krishna, I. Colak, Advances in biomedical applications of Raman microscopy and data processing: a mini review, Anal. Lett. 56 (4) (2023) 576–617, https://doi.org/10.1080/00032719.2022.2094391.
[16] X. Wang, S.-C. Huang, S. Hu, S. Yan, B. Ren, Fundamental understanding and applications of plasmon-enhanced Raman spectroscopy, Nat. Rev. Phys. 2 (5) (2020) 253–271, https://doi.org/10.1038/s42254-020-0171-y.
[17] Y.C. Ou, J.A. Webb, C.M. O'Brien, I.J. Pence, E.C. Lin, E.P. Paul, D. Cole, S.H. Ou, M. Lapierre-Landry, R.C. DeLapp, E.S. Lippmann, A. Mahadevan-Jansen, R. Bardhan, Diagnosis of immunomarkers in vivo via multiplexed surface enhanced Raman spectroscopy with gold nanostars, Nanoscale 10 (27) (2018) 13092–13105, https://doi.org/10.1039/c8nr01478g.
[18] S.K. Gahlaut, D. Savargaonkar, C. Sharan, S. Yadav, P. Mishra, J.P. Singh, Sers platform for Dengue diagnosis from clinical samples employing a hand held Raman spectrometer, Anal. Chem. 92 (3) (2020) 2527–2534, https://doi.org/10.1021/acs.analchem.9b04129.
[19] S.J. Mazivila, H.I.S. Nogueira, R.N.M.J. Páscoa, D.S.M. Ribeiro, J.L.M. Santos, J.M.M. Leitão, J.C.G. Esteves da Silva, Portable and benchtop Raman spectrometers coupled to cluster analysis to identify quinine sulfate polymorphs in solid dosage forms and antimalarial drug quantification in solution by aunps-sers with mcrals, Anal. Methods 12 (18) (2020) 2407–2421, https://doi.org/10.1039/D0AY00693A.
[20] S. Brocklehurst, N. Ghousifam, K. Zuniga, D. Stolley, M.N. Rylander, Multilayer in vitro human skin tissue platforms for quantitative burn injury investigation, Bioengineering-Basel 10 (2) (2023) 265, https://doi.org/10.3390/bioengineering10020265.
[21] R.L. Brekke, S.K. Almeland, K.O. Hufthammer, E. Hansson, Agreement of clinical assessment of burn size and burn depth between referring hospitals and burn centres: a systematic review, Burns 49 (3) (2023) 493–515, https://doi.org/10.1016/j.burns.2022.05.007.
[22] A. Karim, K. Shaum, A. Gibson, Indeterminate-depth burn injury-exploring the uncertainty, J. Surg. Res. 245 (2020) 183–197, https://doi.org/10.1016/j.jss.2019.07.063.
[23] H. Hoeksema, K. Van de Sijpe, T. Tondu, M. Hamdi, K. Van Landuyt, P. Blondeel, S. Monstrey, Accuracy of early burn depth assessment by laser Doppler imaging on different days post burn, Burns 35 (1) (2009) 36–45, https://doi.org/10.1016/j.burns.2008.08.011.
[24] D.D.S. Tavares Pereira, M.H.M. Lima-Ribeiro, N.T. de Pontes-Filho, A.M.A. Carneiro-Leão, M.T.S. Correia, Development of animal model for studying deep second-degree thermal burns, J. Biomed. Biotechnol. 2012 (2012) 460841, https://doi.org/10.1155/2012/460841.
[25] X. Feng, R. Shen, J. Tan, X. Chen, Y. Pan, S. Ruan, F. Zhang, Z. Lin, Y. Zeng, X. Wang, Y. Lin, Q. Wu, The study of inhibiting systematic inflammatory response syndrome by applying xenogenic (porcine) acellular dermal matrix on second-degree burns, Burns 33 (4) (2007) 477–479, https://doi.org/10.1016/j.burns.2006.08.011.
[26] N. Giles, S. Rea, T. Beer, F.M. Wood, M.W. Fear, A peptide inhibitor of c-Jun promotes wound healing in a mouse full-thickness burn model, Wound Repair Regen. 16 (1) (2008) 58–64, https://doi.org/10.1111/j.1524-475X.2007.00331.x.
[27] A. Scabbia, L. Trombelli, A comparative study on the use of a HA/collagen/chondroitin sulphate biomaterial (Biostite@) and a bovine-derived HA xenograft (Bio-Oss@) in the treatment of deep intra-osseous defects, J. Clin. Periodontol. 31 (5) (2004) 348–355, https://doi.org/10.1111/j.1600-051X.2004.00483.x.
[28] X. Luo, T. Zeng, S. He, C. Lin, The combined effects of bone marrow-derived mesenchymal stem cells and microporous porcine acellular dermal matrices on the regeneration of skin accessory cells in vivo, J. Burn Care Res. 39 (2018) 481–490, https://doi.org/10.1093/jbcr/irx002.
[29] X. Luo, W.-X. Tian, Y. Huang, X.-L. Wu, L.-H. Li, P. Chen, X.-G. Zhu, Q.-L. Li, J.-H. Chu, Rapid vascularization identification using adaptive gamma correction and support vector machine based on simulated annealing, J. Infrared Millim. Waves 37 (1) (2018) 98–105, https://doi.org/10.11972/j.issn.1001-9014.2018.01.018.
[30] N.L. Morris, A.R. Cannon, X. Li, M.A. Choudhry, Protective effects of PX478 on gut barrier in a mouse model of ethanol and burn injury, J. Leukoc. Biol. 109 (6) (2021) 1121–1130, https://doi.org/10.1002/JLB.3A0820-323RR.
[31] H.P. Buschman, G. Deinum, J.T. Motz, M. Fitzmaurice, J.R. Kramer, A. van der Laarse, A.V. Bruschke, M.S. Feld, Raman microspectroscopy of human coronary atherosclerosis: biochemical assessment of cellular and extracellular morphologic structures in situ, Cardiovasc. Pathol. 10 (2) (2001) 69–82, https://doi.org/10.1016/S1054-8807(01)00064-3.
[32] J.J. Cárcamo-Vega, M.R. Brañes, A.M. Loske, M.M. Campos-Vallette, The influence of the number of shock waves and the energy flux density on the Raman spectrum of collagen type I from rat, Shock Waves 30 (2) (2020) 201–214, https://doi.org/10.1007/s00193-019-00920-4.
[33] J. Marzi, E.M. Brauchle, K. Schenke-Layland, M.W. Rolle, Non-invasive functional molecular phenotyping of human smooth muscle cells utilized in cardiovascular tissue engineering, Acta Biomater. 89 (2019) 193–205, https://doi.org/10.1016/j.actbio.2019.03.026.
[34] A. Synytsya, D. Janstová, M. Šmidová, A. Synytsya, J. Petrtýl, Evaluation of IR and Raman spectroscopic markers of human collagens: insides for indicating colorectal carcinogenesis, Spectrochim. Acta A 296 (2023) 122664, https://doi.org/10.1016/j.saa.2023.122664.
[35] R. Jain, D. Calderon, P.R. Kierski, M.J. Schurr, C.J. Czuprynski, C.J. Murphy, J.F. McAnulty, N.L. Abbott, Raman spectroscopy enables noninvasive biochemical characterization and identification of the stage of healing of a wound, Anal. Chem. 86 (8) (2014) 3764–3772, https://doi.org/10.1021/ac500513t.
[36] A. Pielesz, D. Biniaś, E. Sarna, R. Bobiński, M. Kawecki, J. Glik, A. Klama-Baryła, D. Kitala, W. Łabuś, J. Paluch, M. Kraut, Active antioxidants in ex-vivo examination of burn wound healing by means of IR and Raman spectroscopies-preliminary comparative research, Spectrochim. Acta A 173 (2017) 924–930, https://doi.org/10.1016/j.saa.2016.10.046.
[37] J. De Gelder, K. De Gussem, P. Vandenabeele, L. Moens, Reference database of Raman spectra of biological molecules, J. Raman Spectrosc. 38 (9) (2007) 1133–1147, https://doi.org/10.1002/jrs.1734.